Deformation of drops at low Reynolds number impact

Loren Jørgensen

Deformation of drops at low Reynolds number impact

L. Jørgensen *

Sciences et Ingénierie de la Matière Molle, CNRS, ESPCI Paris, Université PSL, Sorbonne Université, 75005 Paris, France

(Received 21 November 2023; accepted 18 July 2024; published 1 August 2024)

Drop impact experiments are performed with very viscous fluids to propose a description of the drop deformation at low Reynolds number. We focus on a specific case where dimensionless parameters other than the Reynolds number play no role, which means that only kinetic energy and viscous dissipation determine the final deformation. The same situation in the case of a Reynolds number larger than ten has been clarified years ago. The maximum diameter of the spread drop is well described by a 1/5 power law of the Reynolds number only. Here the deformation of the drop, defined as the contact diameter rescaled by the drop size, is also a power law of the Reynolds number. From experimental data and scaling arguments, the exponent of the power law is shown to be 1/3.

DOI: 10.1103/PhysRevFluids.9.083601

I. INTRODUCTION

Drop impact has been a very popular research field for decades and is still very active. This is mainly due to the ubiquity of natural and industrial phenomena involving drop impact, and also to the fascinating diversity of parameters and outcomes in an apparently very simple system. Without trying an extensive review of the field (see the reviews by Yarin [1], Josserand and Thoroddsen [2] or Wang *et al.* [3]), we can mention works focusing on the drop fluid properties, like surface tension [4–6] or rheology [7–10]; on the impact cinematics, like velocity [11,12] or drop size [13]; on the impacted surface properties, like hydrophobicity [14,15] or texture [16,17]; and even ambient air pressure [18,19] or surface temperature [20,21]. Outcomes include spreading, splashing, receding, or bouncing [1,22], each of those cases being divided in several varieties. Experiments are supported by numerous models and simulations at different scales. Yet there remains some situations that have not been described, despite being common in real life, like small deformation after impact.

The present article thus focuses on drops of very viscous Newtonian liquids, where spreading is driven by kinetic energy only, which is fully dissipated by viscous shear. The parameters are the impact velocity V, the fluid density ρ, viscosity η, and surface tension σ, and the diameter of the drop D_0. Many experimental and theoretical works have studied the maximum spreading state after impact in the framework of purely viscous dissipation [23–27]. Different models have been proposed to describe either the maximum diameter or the minimal thickness as a function of dimensional numbers such as the Reynolds number $\mathrm{Re} = \rho V D_0/\eta$ and the Weber number $\mathrm{We} = \rho V^2 D_0/\sigma$. A few studies also include the dynamic contact angle of the liquid on the solid substrate as a parameter. The different models account for more or less detailed phenomena, but they are not easy to discriminate because the parameters range accessible experimentally is limited. However, when surface tension and wetting can be neglegted and in the simplest approximation that fits experimental data, the maximum spreading factor $\beta_{\max} = D_{\max}/D_0$ [see Figs. 1(a) and 1(b) for notations] is well described by the relation $\beta_{\max} \propto \mathrm{Re}^{1/5}$.

*Contact author: loren.jorgensen@espci.fr

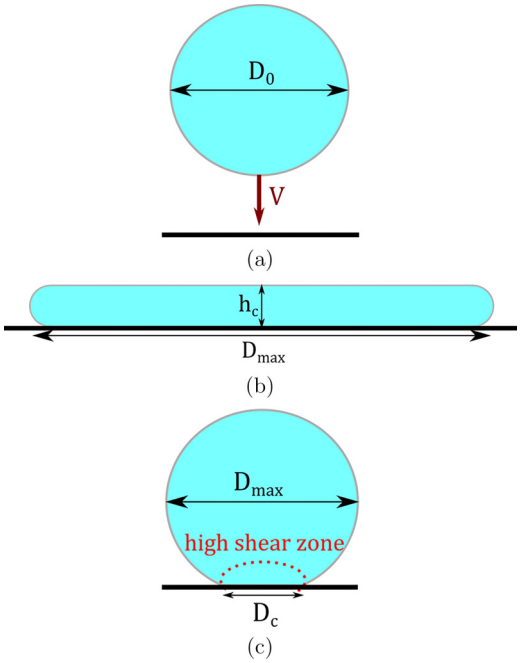

FIG. 1. (a) Drop before impact. (b) Drop in its maximum spreading state with Re $\gg 1$. (c) Drop in its maximum spreading state with Re $\ll 1$.

The relation, even in such a simple version, is very robust in common experimental conditions, but it is worth noticing that all available data restrict to Reynolds numbers above ten, corresponding to a pancake-shape final state.

In the literature, the deformation of impacting drops at lower Reynolds numbers is not described, except in rare studies where several dimensionless numbers play a role simultaneously [15]. This regime can yet be encountered, for example, in concentrated suspension drops [28] or extremely viscous liquid "drops" like molten glass, lava, tar, or pitch.

The present article shows new drop impact experiments where the Reynolds number is varied down to Re $= 0.04$, and proposes a scaling law to describe the inertial spreading of very viscous drops.

II. EXPERIMENTAL METHODS

The viscous liquids are chosen considering that they must be Newtonian, i.e., purely viscous even at the timescale of impact (a few milliseconds), and viscous enough to reach the lowest possible Reynolds number. We use UCON 75-H-90000, a polyalkyleneglycol-based synthetic lubricant produced by Dow for industrial purposes and poly(ethylene-glycol-ran-propylene-glycol)monobutyl ether (denoted PEG for simplicity) from Sigma-Aldrich. They are fully miscible with water, giving access to fluids of various viscosities. Being polymers, they cannot be strictly Newtonian: they are expected to exhibit some viscoelastic features, but it was checked that in our experimental conditions viscoelasticity does not play any role. Details about the rheology measurements supporting that statement can be found in the Appendix. Table I summarizes the main physical properties of the fluids used. Liquid density and surface tension change slightly from one liquid to another, but in the following, for simplicity, each liquid is referred to by its viscosity only. Of course, all values of Table I are taken into account in data analysis.

The drops are produced by forming pendent drops at the tip of a syringe needle, and waiting for spontaneous necking and detachment. Still in the aim of reaching the smallest possible Reynolds

TABLE I. Physical properties of the liquids used. The percentages indicate the mass fraction of UCON or PEG in the mix with water.

Liquid	Viscosity (Pa s) ±5 %	Density (kg/m^3) ±5 kg/m^3	Surface tension (mN/m) ±0.5 mN/m
UCON (pure)	45	1087	40
UCON 80%	17.3	1089	41
UCON 50%	1.13	1070	45
PEG (pure)	2.4	1056	36
PEG 75%	1.02	1068	36.5
PEG 60%	0.37	1064	37
PEG 50%	0.155	1056	38
PEG 45%	0.100	1050	38.5
PEG 35%	0.047	1043	40.5

number, the smallest drops are the most desirable, but using very narrow needles and very viscous liquids requires a large pressure. Bevelled tip needles turn out to be useful in that case because the drop slowly creeps to the bevel tip where it can form a very narrow neck whatever its volume and the internal diameter of the needle. The drop diameter ranges from 1.7 mm to 4.6 mm. Impact velocity is obtained varying the fall height from 0.5 cm to 80 cm, and ranges from 0.09 $m\,s^{-1}$ to 4.0 $m\,s^{-1}$. The target surface is a plain glass slide. The impact zone is illuminated with an intense LED backlight panel and images are recorded from the side with a fast imaging camera Photron Fastcam equipped with a Sigma macro objective. The room temperature is regulated at 20 °C and the drop free fall zone is protected from air motion with cardboard screens.

Several hundreds of drop impacts were performed, changing the liquid, the needle, or the fall height. Each drop impact was analyzed separately: V and D_0 were measured on the recorded images using the software ImageJ. Figure 2 shows different typical examples of drop deformation, at different Reynolds numbers. Corresponding movies can be seen in the Supplemental Material [29].

The first level of analysis consists in checking the conditions required to restrict the study to purely inertioviscous impacts, as defined in the introduction. Therefore, several criteria based on dimensionless numbers are used to select data for further analysis.

The first criterium constrains the minimum impact velocity, linked to the size of the drop. The kinetic energy indeed has to dominate the weight potential energy at contact, to avoid multiple spreading causes at the same time. This corresponds to imposing a lower bound to the Froude number $\mathrm{Fr} = V/\sqrt{gD_0} > 5$, or equivalently, a fall height of at least $12.5D_0$.

The second constraint limits the capillary number $\mathrm{Ca} = \eta V/\sigma$ to values much greater than one, ensuring no effect of wetting at the impact timescale $\tau_i \approx D_0/V$. According to a work by Eddi *et al.* [30], where they study the effect of viscosity on the initial spreading dynamics of drops (without initial velocity), the characteristic time of capillary spreading in that case is $\tau_c = 2\pi\eta D_0/\gamma = 2\pi\mathrm{Ca}\tau_i$. In other words, the spreading due to the impact energy is much faster than the expected wetting velocity if $\mathrm{Ca} \gg 1$. In practice, data where $\mathrm{Ca} < 10$ was discarded. The recordings indeed evidence a first inertial deformation stage over a few milliseconds at most, and then a much slower stage, over a timescale of 100 ms or more, corresponding to gravity- and wetting-driven spreading. Therefore, in the inertial stage, wetting is completely screened, then the surface's nature and roughness do not play any role. Moreover, the capillary number is exactly the ratio of the Weber number and the Reynolds number, then the high values also ensure that viscous dissipation dominates over increase of surface energy.

A qualitative observation of the images raises the question of defining the spreading factor thoroughly to describe the deformation. What is meant by deformation in this work is a

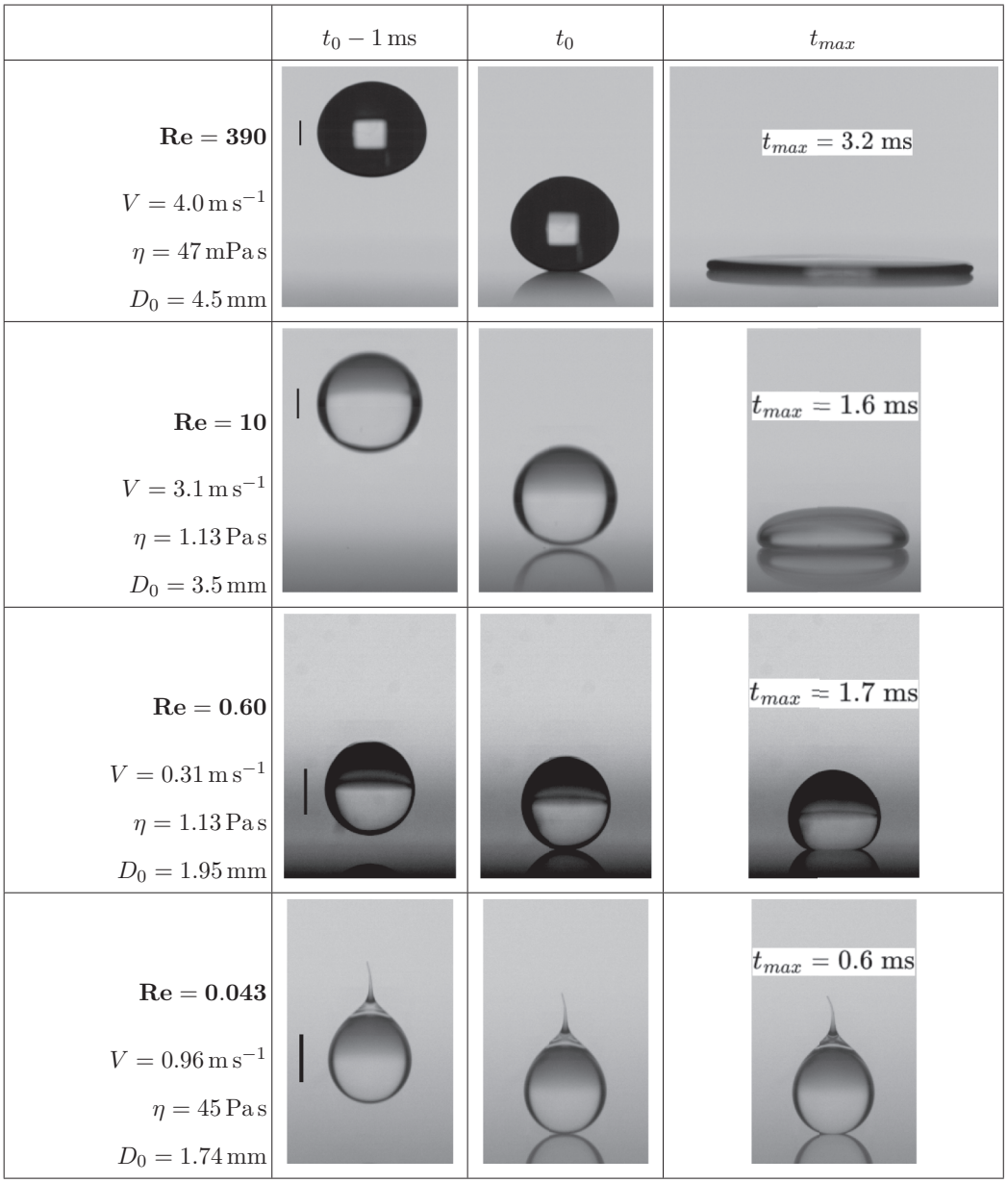

FIG. 2. Typical deformation upon impact of drops with Re = 390, 10, 0.60, and 0.043, respectively. The vertical bars represent 1 mm. The left column is 1 ms before contact, the second one is contact (t_0), and the third one is the maximum spreading, with the corresponding time $t_{\max}$. For each example, the full movie can be seen in the Supplemental Material [29].

descriptor of a change of the drop's shape between the contact time (t_0 in Fig. 2) and the time of full dissipation of initial kinetic energy ($t_{\max}$ in Fig. 2). Usually, the spreading factor is defined as $\beta_{\max} = D_{\max}/D_0$. Strictly, the correct definition is $\beta_{\max} = (D_{\max}/D_0) - 1$ because the initial diameter is substracted from the maximum equator diameter, and then $\beta_{\max}$ does vanish in the limit of no deformation. Still, the -1 is generally neglected because the deformation is large, i.e., $\beta_{\max} \gg 1$. In our case of low deformation, "forgetting" the -1 is not possible. Moreover the

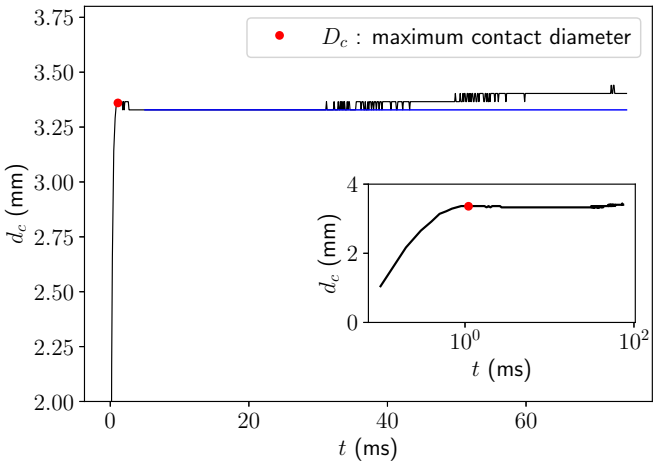

FIG. 3. Typical evolution of the contact diameter, denoted d_c, versus time, for a drop of UCON 50% of initial diameter 2.77 mm impacting at 2.9 m/s. The capillary number is Ca = 73. The blue horizontal line is a guide for the eyes. The red dot represents D_c, the contact diameter at the maximum inertial spreading state of the drop. Inset: same curve in semilogarithmic scale to focus on the short timescale.

image resolution is not good enough to actually detect a difference between D_0 and $D_{\max}$. Therefore, we made a different choice to quantify the deformation. Instead of the maximum equator diameter $D_{\max}$, we measure the maximum contact diameter D_c [see Figs. 1(c) and 3] and define a different spreading factor $\beta_{\max} = D_c/D_0$. As D_c ranges from 0 to $\approx D_0$ at low deformation, the relative error due to image resolution is reduced. This definition also provides a continuous description of both low deformation and high deformation, because in the pancake shape $D_{\max}$ and D_c are nearly identical.

Figure 3 shows a typical example of the contact diameter evolution in time, and illustrates the definition of D_c. The neat separation between timescales, visible on the recordings, is also confirmed.

Another detail can be seen on the images. A large proportion of the drops do not have a spherical shape before impact, due to the time needed to relax after detachment. They rather have an elongated pear shape with a more or less pronounced tail (see the last line of Fig. 2). The shape relaxation time is approximately $\tau_{sh} \approx \eta d/\gamma$ with d the typical width of the tail. In comparison, the drop falling time is $\tau_f \approx V/g$ (g is the acceleration of gravity). The two times are often comparable, and for the most viscous fluids and the smallest velocities, the falling time is shorter than the relaxation time of the tail. As this happened for the drops with the lowest Reynolds numbers, it was necessary to make sure that the shape of the initial drop does not change the results, and if so, to take the difference into account. A recent work on viscoplastic drop impacts [31] underlines the strong effect of the drop aspect ratio on the final deformation, but the effect seems to correspond to the increase of the drop's mass and then of its kinetic energy. Therefore, we also compute the actual volume $\mathcal{V}$ of each drop from their outline. The Reynolds number used in the plot of Fig. 4 is then not exactly as defined in the introduction, but multiplied by the ratio of the actual volume and the volume of a spherical drop of diameter D_0: $\mathrm{Re} = \rho V D_0/\eta \times \mathcal{V}/(\pi D_0^3/6)$. The validity of this choice also appears in Sec. III.

For quantitative analysis, D_c and $\mathcal{V}$ were also measured on the recorded images, to be able to compute $\beta_{\max}$ and the correction for Re. To check consistence with other data from the literature, values at higher Reynolds number from Lagubeau *et al.* [26] are adapted as follows: the minimum spread drop thickness h_c (normalized by the initial diameter) shown in their paper is transformed into the maximum diameter $D_{\max} \approx D_c$ (also normalized), assuming that the spread drop is a flat cylinder of height h_c and diameter $D_{\max}$. Figure 4 shows $\beta_{\max}$ versus Re. The 1/5 power law is

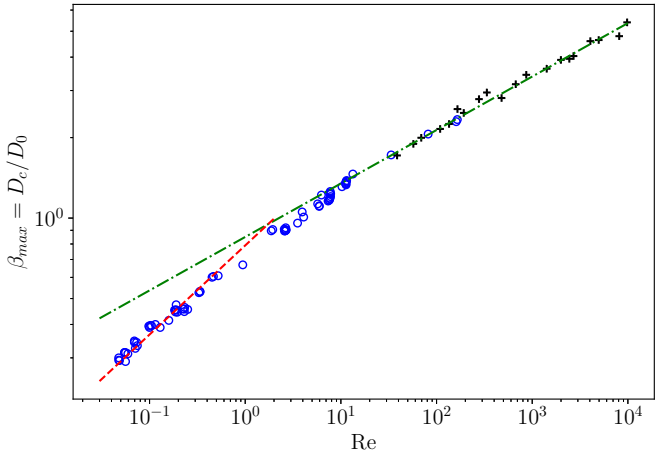

FIG. 4. Deformation $\beta_{\max} = D_c/D_0$ as a function of the Reynolds number (blue circles). Data at higher Reynolds number adapted from Lagubeau *et al.* [26] are also represented (black crosses). The green dashed line is a 1/5 power law and the red dashed line is a 1/3 power law.

also represented and fits well all the data above Re ≈ 10. For lower values of Re < 1, the data still collapse on a master curve, but deviate from the 1/5 power law. In the following we will show that those data follow a 1/3 power law.

III. DIMENSIONAL ANALYSIS

In this section we propose a scaling to describe the deformation of the drop, defined as $\beta_{\max} = D_c/D_0$, as a function of the Reynolds number, for Re < 1. The key idea is an energy balance, all the kinetic energy being dissipated by the viscous shear of a part of the drop only.

The estimation of the extend of the most sheared zone is largely based on the works of Philippi *et al.* [32] and Gordillo *et al.* [33]. During impact of the most viscous drops, deformation is only visible at the bottom of the drop and the top is not affected (see, for example, the two last lines of Fig. 2). This is reminiscent of the early deformation of an inviscid drop, that would keep the shape of a truncated sphere, yielding a contact radius growing as $r_c(t) \sim \sqrt{Vt/D_0}$ [34]. The vertical extend of the sheared zone is supposed to be the thickness of the time-expanding viscous layer introduced as a correction to the autosimilar pressure and velocity fields computed for inviscid drops [23,32,33]. The viscous layer thickness also grows as a square root of time $l_v \sim \sqrt{\eta t/\rho}$. Therefore the volume of the sheared zone grows like D_c^3 at all times. Since both physical ingredients (kinematic deformation and viscous layer) were first developped considering characteristic dimensions much smaller than the drop diameter, the scaling we propose will only apply to deformations $\beta_{\max}$ smaller than one.

Dimensionally, the shear rate is the velocity gradient $\dot{\gamma} \sim V/D_c$ (we recall that the thickness of the viscous boundary layer evolves like D_c) and the shear is the deformation $\gamma \sim D_c/D_0$. The viscous dissipated energy then scales as

$$E_\eta \sim \eta \times \frac{D_c}{D_0} \times \frac{V}{D_c} \times D_c^3.$$

The kinetic energy scales as

$$E_k \sim \rho V^2 D_0^3.$$

Finally,

$$\left(\frac{D_c}{D_0}\right)^3 \sim \frac{\rho V D_0}{\eta} \equiv \mathrm{Re}.$$

Based on that estimation, for $\mathrm{Re} < 1$, the deformation of the drop is described by

$$\beta_{\max} \propto \mathrm{Re}^{1/3}. \tag{1}$$

This power law perfectly fits the data below $\mathrm{Re} \approx 1$ (Fig. 4). Note that only the dependence in Re is predicted by 1, then an adjustable prefactor is used to plot the 1/3 power law in Fig. 4.

The kinetic energy is written considering an initially spherical drop of diameter D_0, which is not the case for the most viscous drops, as explained before. However, the kinetic energy could as well be expressed $E_k \sim \rho V^2 \mathcal{V}$, yielding the same relation (1), with the Reynolds number defined in Sec. II. On the other hand, the argument used to evaluate the energy dissipation is that a small part of the drop only, in the neighborhood of the contact with the substrate, is sheared. Then, as long as the bottom part of the drop is quasispherical with a curvature radius of $D_0/2$, the deformation $\beta_{\max} = D_c/D_0$ is not affected by the shape of the drop's upper half.

IV. CONCLUSIONS

The present work introduces a scaling to describe the deformation of viscous drops upon impact as a function of the drop's Reynolds number Re, when the latter is smaller than one. A similar law already existed for $\mathrm{Re} \gg 1$, where the whole drop is sheared and flattened onto the substrate, but the case of $\mathrm{Re} \ll 1$ had never been described.

To establish the scaling law, we performed drop impact experiments, varying the liquid viscosity, the impact velocity, and the drop diameter. Possible influence of parameters other than the drop's inertia and the viscosity of the fluid has been carefully avoided. The experimental data was properly described by a 1/3 power law obtained through scaling arguments. The key idea to understand the origin of that scaling law is that viscous shear in a reduced fluid volume around the contact zone is enough to dissipate all the kinetic energy.

This result is relevant for a number of situations, especially in earth sciences or industry (granular suspensions, melt glass or rocks, viscous polymer melts, tar). Interestingly, the model does not depend on the shape of the full drop, but only of its bottom part, which undergoes the deformation. The prediction of the contact surface size of such drops can help modelizing more complex situations where the flux of some quantity (like heat) is only significant through the liquid-solid interface.

Future developments of this work could benefit from numerical simulations of the flow field close to the contact line, for example [32], allowing for better estimations of the dissipated energy. The knowledge of the shear distribution would bring crucial information to describe the effects of complex rheology, in particular.

ACKNOWLEDGMENTS

The author wishes to thank H. Lhuissier for the opportunity to start this study as a postdoc researcher in his team, C. Monteux and E. Barthel for useful advice, and C. Barentin for providing a sample of UCON.

APPENDIX: NEWTONIAN APPROXIMATION

To assess the potential influence of viscoelasticity on the experiments, the storage and loss moduli of both fluids were measured by small oscillatory shear with a rheometer (DHR3 from TA Instruments) at the temperature of experiments (20 °C). Standard stress-controlled rheometers generally do not give reliable measurements at higher frequencies, typically above 20 Hz, especially

for low torque signal, because of the internal inertia of the rheometer and geometry. To overcome this issue, the range of frequencies was extended using time-temperature equivalence, and the data were fitted by a simple Maxwell model. This procedure yielded approximative viscoelastic relaxation times of $\tau_v \approx 200\,\mu s$ for pure UCON and $\tau_v \approx 5\,\mu s$ for pure PEG. Even if those values are only estimations, they remain much smaller than the typical impact time for all our data.

The resulting maximal Weissenberg number is $\mathrm{Wi} = \dot{\gamma}\ \tau_v \approx 0.2$, justifying to ignore any viscoelastic effect in the experiments.

[1] A. L. Yarin, Drop impact dynamics: Splashing, spreading, receding, bouncing..., Annu. Rev. **38**, 159 (2006).

[2] C. Josserand and S. Thoroddsen, Drop impact on a solid surface, Annu. Rev. Fluid Mech. **48**, 365 (2016).

[3] X. Wang, B. Xu, S. Guo, Y. Zhao, and Z. Chen, Droplet impacting dynamics: Recent progress and future aspects, Adv. Colloid Interface Sci. **317**, 102919 (2023).

[4] M. Pasandideh-Fard, Y. M. Qiao, S. Chandra, and J. Mostaghimi, Capillary effects during droplet impact on a solid surface, Phys. Fluids **8**, 650 (1996).

[5] C. Clanet, C. Béguin, D. Richard, and D. Quéré, Maximal deformation of an impacting drop, J. Fluid Mech. **517**, 199 (2004).

[6] S. Wildeman, C. W. Visser, C. Sun, and D. Lohse, On the spreading of impacting drops, J. Fluid Mech. **805**, 636 (2016).

[7] V. Bertola, Dynamic wetting of dilute polymer solutions: The case of impacting droplets, Adv. Colloid Interface Sci. **193-194**, 1 (2013).

[8] V. Bertola and M. D. Haw, Impact of concentrated colloidal suspension drops on solid surfaces, Powder Technol. **270**, 412 (2015).

[9] L.-H. Luu and Y. Forterre, Drop impact of yield-stress fluids, J. Fluid Mech. **632**, 301 (2009).

[10] F. Boyer, E. Sandoval-Nava, J. H. Snoeijer, J. F. Dijksman, and D. Lohse, Drop impact of shear thickening liquids, Phys. Rev. Fluids **1**, 013901 (2016).

[11] J. B. Lee, N. Laan, K. G. de Bruin, G. Skantzaris, N. Shahidzadeh, D. Derome, J. Carmeliet, and D. Bonn, Universal rescaling of drop impact on smooth and rough surfaces, J. Fluid Mech. **786**, R4 (2016).

[12] H.-M. Huang and X.-P. Chen, Energetic analysis of drop's maximum spreading on solid surface with low impact speed, Phys. Fluids **30**, 022106 (2018).

[13] C. W. Visser, P. E. Frommhold, S. Wildeman, R. Mettin, D. Lohse, and C. Sun, Dynamics of high-speed micro-drop impact: Numerical simulations and experiments at frame-to-frame times below 100 ns, Soft Matter **11**, 1708 (2015).

[14] J. B. Lee, D. Derome, R. Guyer, and J. Carmeliet, Modeling the maximum spreading of liquid droplets impacting wetting and nonwetting surfaces, Langmuir **32**, 1299 (2016).

[15] S. Lin, B. Zhao, S. Zou, J. Guo, Z. Wei, and L. Chen, Impact of viscous droplets on different wettable surfaces: Impact phenomena, the maximum spreading factor, spreading time and post-impact oscillation, J. Colloid Interface Sci. **516**, 86 (2018).

[16] L. Xu, Liquid drop splashing on smooth, rough, and textured surfaces, Phys. Rev. E **75**, 056316 (2007).

[17] P. Tsai, M. H. W. Hendrix, R. R. M. Dijkstra, L. Shui, and D. Lohse, Microscopic structure influencing macroscopic splash at high Weber number, Soft Matter **7**, 11325 (2011).

[18] C. S. Stevens, A. Latka, and S. R. Nagel, Comparison of splashing in high- and low-viscosity liquids, Phys. Rev. E **89**, 063006 (2014).

[19] E. Q. Li, K. R. Langley, Y. S. Tian, P. D. Hicks, and S. T. Thoroddsen, Double contact during drop impact on a solid under reduced air pressure, Phys. Rev. Lett. **119**, 214502 (2017).

[20] T. Tran, H. J. J. Staat, A. Prosperetti, C. Sun, and D. Lohse, Drop impact on superheated surfaces, Phys. Rev. Lett. **108**, 036101 (2012).

[21] J. Breitenbach, I. V. Roisman, and C. Tropea, From drop impact physics to spray cooling models: A critical review, Exp Fluids **59**, 55 (2018).
[22] R. Rioboo, C. Tropea, and M. Marengo, Outcomes from a drop impact on solid surfaces, Atomiz. Spr. **11**, 12 (2001).
[23] I. V. Roisman, Inertia dominated drop collisions. II. An analytical solution of the Navier–Stokes equations for a spreading viscous film, Phys. Fluids **21**, 052104 (2009).
[24] R. D. Schroll, C. Josserand, S. Zaleski, and W. W. Zhang, Impact of a viscous liquid drop, Phys. Rev. Lett. **104**, 034504 (2010).
[25] J. Eggers, M. A. Fontelos, C. Josserand, and S. Zaleski, Drop dynamics after impact on a solid wall: Theory and simulations, Phys. Fluids **22**, 062101 (2010).
[26] G. Lagubeau, M. A. Fontelos, C. Josserand, A. Maurel, V. Pagneux, and P. Petitjeans, Spreading dynamics of drop impacts, J. Fluid Mech. **713**, 50 (2012).
[27] N. Laan, K. G. de Bruin, D. Bartolo, C. Josserand, and D. Bonn, Maximum diameter of impacting liquid droplets, Phys. Rev. Appl. **2**, 044018 (2014).
[28] L. Jørgensen, Y. Forterre, and H. Lhuissier, Deformation upon impact of a concentrated suspension drop, J. Fluid Mech. **896**, R2 (2020).
[29] See Supplemental Material at http://link.aps.org/supplemental/10.1103/PhysRevFluids.9.083601 for videos (AVI format) of the 4 examples shown in Fig. 2. The Reynolds number is given again in the filename.
[30] A. Eddi, K. G. Winkels, and J. H. Snoeijer, Short time dynamics of viscous drop spreading, Phys. Fluids **25**, 013102 (2013).
[31] K. Isukwem, J. Godefroid, C. Monteux, D. Bouttes, R. Castellani, E. Hachem, R. Valette, and A. Pereira, The role of viscoplastic drop shape in impact, J. Fluid Mech. **978**, A1 (2024).
[32] J. Philippi, P.-Y. Lagrée, and A. Antkowiak, Drop impact on a solid surface: Short-time self-similarity, J. Fluid Mech. **795**, 96 (2016).
[33] L. Gordillo, T.-P. Sun, and X. Cheng, Dynamics of drop impact on solid surfaces: Evolution of impact force and self-similar spreading, J. Fluid Mech. **840**, 190 (2018).
[34] R. Rioboo, M. Marengo, and C. Tropea, Time evolution of liquid drop impact onto solid, dry surfaces, Exp. Fluids **33**, 112 (2002).